Available online at website: https://journal.bcrec.id/index.php/bcrec

Bulletin of Chemical Reaction Engineering & Catalysis, 20 (2) 2025, 346-358

Original Research Article

Nigella Sativa-mediated Synthesis of $BiVO_4$/g-C_3N_4 Composites for the Removal of Methylene Blue Dye

Ghinatanitha Haqqu Haryadinaru, Tien Setyaningtyas, Anung Riapanitra*

Chemistry Department, Faculty of Mathematics and Natural Sciences, Jenderal Soedirman University, Purwokerto, 53122, Indonesia

Received: 13th February 2025; Revised: 21th April 2025; Accepted: 22th April 2025
Available online: 26th April 2025; Published regularly: August 2025

Abstract

This study investigates the synthesis and photocatalytic performance of $BiVO_4$-Nigella Sativa/g-C_3N_4 composites for the degradation of methylene blue dye. The composites were synthesized using a coprecipitation method and characterized through various techniques, including X-ray diffraction (XRD), Fourier-transform infrared spectroscopy (FTIR), UV-Vis diffuse reflectance spectroscopy (DRS), Brunauer-Emmett-Teller (BET) surface area analysis, and scanning electron microscopy (SEM) to determine their crystal structure, chemical composition, morphology, adsorption and photocatalytic abilities. A variation of mass ratios of $BiVO_4$ to g-C_3N_4 of 1:2, 1:3, and 1:4 was used in this investigation. The photocatalytic test results indicated that the composite with a mass ratio of 1:2 achieved the highest methylene blue degradation, reaching 91.73%, which was primarily attributed to an adsorption activity of 81.12% and a photocatalytic degradation of 10.60%. The photocatalytic activity was significantly enhanced under alkaline conditions, particularly at pH levels between 9 and 10, which facilitated the formation of reactive oxygen species (ROS). The study highlights the synergistic effects of the $BiVO_4$ and g-C_3N_4 combination, which promotes efficient charge transfer, reduces electron-hole recombination, and expands light absorption due to a decrease in the effective bandgap energy. Overall, the findings indicate that $BiVO_4$-Nigella Sativa/g-C_3N_4 composites have considerable potential for application in wastewater treatment, particularly for the remediation of organic dye pollutants.

Keywords: Photocatalysis; BiVO4; Nigella Sativa; g-C3N4; Methylene blue; Adsorption

How to Cite: Haryadinaru, G. H., Setyaningtyas, T., Riapanitra, A. (2025). Nigella Sativa-mediated Synthesis of $BiVO_4$/g-C_3N_4 Composites for the Removal of Methylene Blue Dye. *Bulletin of Chemical Reaction Engineering & Catalysis*, 20 (2), 346-358. (doi: 10.9767/bcrec.20354)

Permalink/DOI: https://doi.org/10.9767/bcrec.20354

1. Introduction

Water pollution due to industrial waste effluents, especially from the textile, pharmaceutical, and paper sectors, is one of the most serious environmental challenges [1]. These effluents often contain dyes such as methylene blue (MB), which are toxic and difficult to degrade naturally. These persistent dyes pose significant threats to aquatic ecosystems and human health. Therefore, effective and environmentally friendly effluent treatment methods are needed to overcome this problem [2]. Some physicochemical methods such as adsorption and coagulation require further treatment as they do not degrade the dye. One promising method is photodegradation, which degrades organic compounds using light energy with the help of photocatalyst materials. Titanium dioxide is the most prominent photocatalyst due to its high photocatalytic activity under. It is, however, absorbs UV light wavelength, limiting its application [3]. Bismuth vanadate ($BiVO_4$) has been widely studied as a photocatalyst because it has a semiconductor bandgap of about 2.4 eV, allowing visible light absorption. In addition, $BiVO_4$ has good chemical stability and high

* Corresponding Author.
Email: anung.riapanitra@unsoed.ac.id (A. Riapanitra)

oxidizing properties [4]. However, the main limitation of $BiVO_4$ is the high recombination rate of electron-hole pairs, which reduces its photocatalytic efficiency [5].

Various efforts have been made to improve the performance of $BiVO_4$, one of which is through modification with natural materials such as the use of Callistemon viminalis [6]. Nigella Sativa (NS) seed is a natural material rich in bioactive compounds, such as alkaloids, flavonoids, and tannins, which can function as morphology controllers in material synthesis [7]. Based on previous studies, using natural materials in the synthesis process can affect the crystal structure, morphology and produce photocatalysts with smaller particle sizes and larger surface areas, thereby improving the degradation efficiency of organic pollutants [8]. Researchers have also enhanced $BiVO_4$ photocatalysts through elemental doping and semiconductor coupling to improve charge separation and photocatalytic activity, and one of the prominent candidates is graphitic carbon nitride (g-C_3N_4). g-C_3N_4 is a carbon-based polymeric material with a graphitic structure and a bandgap of about 2.7 eV. Although the bandgap of g-C_3N_4 is higher than that of $BiVO_4$, this material can separate electron-hole pairs and has high thermal and chemical stability [9]. Compositing $BiVO_4$ with g-C_3N_4 can form a heterojunction, facilitating charge transfer between materials. Based on previous research, this heterojunction not only enhances the separation of electron-hole pairs but also lowers the effective bandgap of the composite system, thereby broadening the spectrum of light that can be absorbed [10].

The use of $BiVO_4$/g-C_3N_4 composites has proven effective in degrading organic pollutants under visible light. Mu *et al.* studied S-scheme $BiVO_4$/g-C_3N_4 heterojunctions for peroxydisulfate-activated degradation of dissolved organic matter in eutrophic lake water, achieving 85% degradation in 120 minutes [11]. Tran et al. investigated a Z-scheme $BiVO_4$/g-C_3N_4 heterostructure for dye and antibiotic decomposition, achieving 95% methylene blue and 88% rhodamine B degradation in 90 minutes. The Z-scheme mechanism improved charge carrier dynamics, optimizing redox species generation for organic degradation[12]. Shakir *et al.* explored tungsten-doped $BiVO_4$/g-C_3N_4 composites, achieving 80% phenol degradation in 180 minutes under visible light. Tungsten doping enhanced electronic properties and material interaction, boosting photocatalytic efficiency [13]. Also, Akechatree et al. developed a Z-scheme $BiVO_4$/g-C_3N_4/rGO nanocomposite, achieving over 92% degradation of methylene blue and tetracycline in 120 minutes. The inclusion of rGO and g-C_3N_4 improved charge separation and pollutant adsorption, increasing photocatalytic activity by 25% compared to $BiVO_4$/g-C_3N_4 alone [14].

To enhance the performance of $BiVO_4$, it was composited with Graphitic carbon nitride (g-C_3N_4) material. This research aims to synthesize and characterize $BiVO_4$ photocatalyst modified with NS extract and composite it with g-C_3N_4. The evaluation of photocatalyst performance is performed through methylene blue degradation testing, with the hope that the results of this study can contribute to the development of efficient and environmentally friendly photocatalytic-based waste treatment technology.

2. Materials and Methods

2.1 Materials

The materials used in this study include NS seed extract, which was obtained from black cumin seeds, bismuth(III) nitrate pentahydrate ($Bi(NO_3)_3$-$5H_2O$) (Merck, Germany), ammonium metavanadate (NH_4VO_3) (Aldrich, USA), sodium hydroxide (NaOH) (Merck, Germany), and melamine (Loba Chemie, Germany). Methylene blue dye (Merck, Germany), demineralized water, and distilled water were also used in the synthesis and testing process. For other experimental purposes, methanol (Merck, Germany), absolute ethanol (Merck, Germany), hydrochloric acid (HCl) (Merck, Germany), as well as radical-forming compounds, such as benzoquinone (Aldrich, USA), isopropanol (Merck, Germany), and ammonium oxalate (Merck, Germany), were used. The instruments used were Shimadzu XRD-7000 X-ray Diffractometer (XRD), JEOL JSM-6510LA Scanning Electron Microscope (SEM), Hitachi U-3010 UV-Visible Diffuse Reflectance Spectroscopy (UV-Vis DRS) spectrophotometer and Brunauer-Emmett-Teller (BET) Quantachrome Nova 1200e surface area analyzer.

2.2 Preparation of $BiVO_4$ via NS

Black cumin seeds were first rinsed with distilled water and air-dried. A total of 10 g of black cumin seeds were weighed and ground into a fine powder using a clean mortar and pestle and placed in a three-necked flask. The seeds were then heated in 400 mL of deionized water at 100°C for 2 hours with constant stirring. After heating, the solution was allowed to cool to room temperature. The brownish NS extract was then filtered using Whatman No. 1 filter paper to separate the solution from the solid residue, resulting in a clear filtrate ready for further synthesis without further dilution or concentration.

A 1.936 g $Bi(NO_3)_3$-$5H_2O$ was dissolved in 8 mL of NS seed extract to form solution one. Solution two was prepared by dissolving 0.468 g NH_4VO_3 in 8 mL NS extract. Solution one was

slowly added to solution two while stirring with a magnetic stirrer for 2 hours at room temperature. The mixture produced a yellow solution, which was then centrifuged. The precipitate obtained was washed three times with ethanol and demineralized water. The produced $BiVO_4$ powder was then calcined at 400 °C for 4 hours. This procedure is modification of previous researcher [1].

2.3 Preparation of $BiVO_4$-NS/g-C_3N_4

$BiVO_4$-NS/g-C_3N_4 composites were prepared in two steps. After successfully synthesizing $BiVO_4$-NS, g-C_3N_4 was prepared using a thermal condensation method. A total of 5 g of melamine was placed in a closed alumina crucible and heated to 550 °C, which was maintained for 4 hours. After cooling to room temperature, the g-C_3N_4 product was pulverized into fine powder and then used to form the $BiVO_4$-NS/g-C_3N_4 composite. A total of 0.2 g g-C_3N_4 was dispersed in 20 mL of methanol; then, the mixture was stirred ultrasonically for 1 hour to exfoliate the g-C_3N_4. Afterward, 0.1 g $BiVO_4$ was added into the g-C_3N_4 suspension, and the mixture was stirred using a magnetic stirrer in a fume hood until the methanol evaporated completely. The $BiVO_4$-NS/g-C_3N_4 composite photocatalyst was dried at 80 °C and calcined at 300 °C for 4 hours. This procedure was repeated for samples with a $BiVO_4$-NS:g-C_3N_4 mass ratio of 1:3 and 1:4. This procedure is modification of previous researcher [1].

2.4 Photocatalyst Material Characterization

Characterization of photocatalyst materials is performed using various techniques to identify their properties. X-ray diffraction (XRD) analysis using a Shimadzu XRD-7000 was used to determine the crystal structure and phase of the material from the resulting diffraction pattern. A JEOL JSM-6520LA scanning electron microscope (SEM) was used to examine the surface morphology by scanning the sample with an electron beam to produce images showing particle size and shape. In addition, Fourier Transform Infrared (FTIR) spectrum analysis was performed to identify functional groups and chemical interactions in the material. UV-Vis diffuse reflectance spectroscopy (UV-Vis DRS) using a JASCO V-670 was used to measure the ability of the material to absorb UV and visible light and to determine the band gap energy. Brunauer-Emmett-Teller (BET) analysis was used to evaluate the specific surface area and pore size distribution, which play an essential role in the photocatalytic activity of the material.

2.5 $BiVO_4$-NS /g-C_3N_4 Photocatalyst Optimization

The optimization process of photocatalyst mass and pH for methylene blue (MB) degradation was carried out in two steps. At first, 0.05 g of $BiVO_4$-NS/g-C_3N_4 photocatalyst with different mass ratios of 1:2, 1:3, and 1:4 was mixed into 50 mL of 10 ppm MB solution in a glass beaker. The mixture was stirred while exposed to visible light for 150 minutes. The absorbance of the solution was measured using a UV-Vis spectrophotometer to determine the photocatalyst ratio that gave the best performance in MB degradation.

The next step was to adjust the pH of the solution. A 50 mL solution of 10 ppm MB was added to a beaker, and the pH was adjusted to values of 3, 5, 7, 9, and 11. The mixture was stirred under visible light for a predetermined time. Absorbance measurements were taken to determine the optimal pH that resulted in the highest MB degradation.

3. Results and Discussion

3.1 Crystalline Phase Identification of $BiVO_4$-NS/g-C_3N_4

The XRD results presented in Figure 1 for the three samples of g-C_3N_4, $BiVO_4$ NS seed extract, and the $BiVO_4$-NS/g-C_3N_4 composite offer detailed insights into the changes in crystallinity following composite formation. The diffraction pattern of $BiVO_4$-NS seed extract showed sharp and well-defined diffraction peaks, such as in the (011), (121), (130), and (040) crystal planes in accordance with the standard values (JCPDS No. 14-0688) [15]. These peaks are typical for the monoclinic crystal structure of $BiVO_4$, indicating that the material has high crystallinity and good order. The presence of NS in $BiVO_4$ is not expected to introduce new peaks, as organic components like NS are typically amorphous and lack the crystalline regularity detectable by XRD.

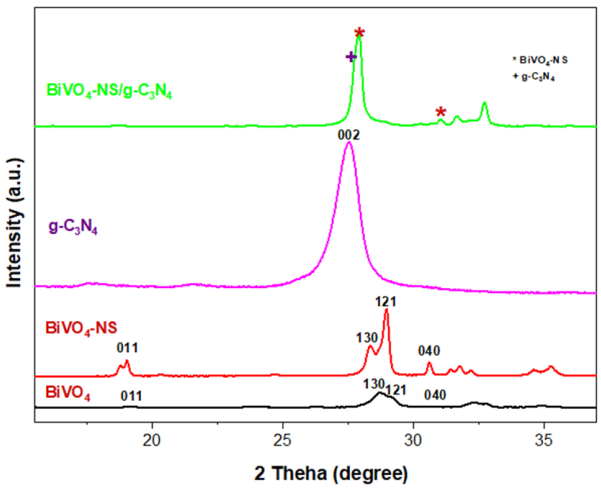

Figure 1. X-ray diffraction characterization

However, NS seed extract may act as a supporting agent that affects the particle size or morphology of the material, although this is not directly reflected in the diffraction pattern [16].

Meanwhile, g-C_3N_4, as a layer-structured material, exhibits a dominant diffraction peak in the (002) plane around $2\theta = 27.4°$, representing the distance between graphitic layers [17]. This peak is the only significant peak observed in the XRD pattern of g-C_3N_4, indicating that the material has a semi-crystalline structure with a layered nature. This interlayer stacking is characteristic of g-C_3N_4 and implies successful hybridization with $BiVO_4$. When the two materials, $BiVO_4$-NS and g-C_3N_4, were combined in composite form, there was a significant change in the diffraction pattern. The sharp peaks of $BiVO_4$-NS that were previously clearly visible began to show intensity attenuation and broadening. This indicates that the formation of the composite caused a reduction in the size of the $BiVO_4$-NS crystal domains, which in turn affected the intensity of the diffraction peaks. The broadening of the peaks can also be caused by disrupting the $BiVO_4$-NS crystal order due to the presence of g-C_3N_4.

Furthermore, the peak corresponding to g-C_3N_4 in the (002) plane is also noticeably weakened in the composite diffraction pattern. This weakening indicates that the interaction between $BiVO_4$-NS and g-C_3N_4 is strong enough to disrupt the stacking of g-C_3N_4 layers. In the composite, $BiVO_4$-NS particles tend to be dispersed on the surface of g-C_3N_4, which limits the interaction between g-C_3N_4 layers and decreases the intensity of its XRD peaks. The presence of NS as an organic component does not result in a detectable XRD signal. Still, it most likely contributes indirectly by facilitating particle distribution or acting as a stabilizing agent. NS may also strengthen interactions between particles, enhancing the formation of unique composite networks.

Based on Table 1, the crystallite sizes obtained from XRD analysis using Scherrer's formula show significant variations among the g-C_3N_4, $BiVO_4$-NS, and $BiVO_4$-NS/g-C_3N_4 composites. The g-C_3N_4 material has the smallest crystallite size of 6.52 nm, which reflects a material structure with low crystallinity and small particle size. $BiVO_4$-NS has a larger crystallite size of 16.78 nm, indicating a more ordered crystal structure than g-C_3N_4. When the two materials were combined into a $BiVO_4$-NS/g-C_3N_4 composite, the crystal size increased to 20.09 nm.

Table 1. Photocatalyst material crystal size

Sample	Crystal Size (nm)
g-C_3N_4	6.52
$BiVO_4$-NS	16.78
$BiVO_4$-NS/g-C_3N_4	20.09

This increase can be attributed to the interaction between the two materials during the synthesis process, where g-C_3N_4 can act as a matrix for the formation of $BiVO_4$-NS particles. It could also indicate the presence of larger crystal growth or particle coalescence during the composite synthesis process. Despite the larger crystal size of the composite, this is not always a drawback. In some cases, synergistic interactions between the two materials can improve material characteristics, such as charge transfer efficiency and structural stability [18]. Overall, the changes in diffraction patterns and increase in crystal size indicate the successful formation of composites with synergistic interactions. These changes increase the surface area, particle distribution, and availability of active sites, which contribute to the efficiency of charge transfer and light utilization, thus supporting the improvement of the photocatalytic performance of the material.

Furthermore, no impurity phases were detected, indicating high phase purity of the composites. The preservation of individual phase structures alongside the absence of secondary phases suggests that the heterojunction is formed via physical integration rather than chemical transformation, which is beneficial for maintaining the intrinsic band structure alignment necessary for efficient photocatalytic activity.

3.2 Functional Group and Chemical Bond Identification

The FTIR spectra provides important information regarding the functional groups in the BiVO4-NS, g-C3N4, and BiVO4-NS/g-C3N4 composite materials. Figure 2 shows that the FTIR spectrum of $BiVO_4$-NS shows various characteristic peaks that reflect the presence of specific functional groups. The peak at around 3400 cm^{-1} indicates the presence of O–H stretching vibrations, which originate from adsorbed water or hydroxyl groups on the surface of the material. In addition, peaks in the 3000-2850 cm^{-1} region show aliphatic C–H stretching vibrations, indicating the presence of residual organic residues from NS. C=O stretching vibrations were detected around 1700-1600 cm^{-1}, indicating the presence of carbonyl groups derived from organic compounds.

The peak at 1380 cm^{-1} indicates the presence of nitrate ions (NO^{3-}), which may come from the nitrate-based reagents used in the synthesis. Meanwhile, the characteristic V–O vibrations at

800-900 cm^{-1} and Bi–O at 500-600 cm^{-1} are typical of the $BiVO_4$ crystal structure. The presence of these peaks confirmed that the crystalline phase of $BiVO_4$ was successfully formed and maintained in the $BiVO_4$ -NS composite [19,20].

In the spectrum of $BiVO_4$-NS/g-C_3N_4, no new peaks were observed in the spectrum of pure $BiVO_4$-NS, indicating the successful formation of the composite. The peaks at 3000-3500 cm^{-1} indicate wider O–H stretching caused by the interaction of hydroxyl groups on the surface of g-C_3N_4 with the surrounding environment. A key characteristic of g-C_3N_4 is the presence of C=N groups indicated by peaks around 1200-1600 cm^{-1}. This group is characteristic of the triazine ring in g-C_3N_4, which contributes to the aromatic structure of the material. In addition, strong C–N stretching vibrations were detected at around 1100 cm^{-1}, indicating the presence of nitrogen-carbon heteroatom chains. Peaks at 2800-3000 cm^{-1} indicating aliphatic C–H stretching vibrations also indicate organic residues from NS or even impurities from the solvent used during synthesis. Interestingly, the characteristic peaks of $BiVO_4$, namely V-O and Bi-O vibrations, remain visible at around 800-900 cm^{-1} and 500-600 cm^{-1} [19]. This indicates that the structure of $BiVO_4$ remains stable despite having formed a composite with g-C_3N_4. Importantly, a noticeable shift or broadening of some bands (especially in the 1200–1650 cm^{-1} region) can be observed in the composite compared to the individual components. This is indicative of interfacial interactions, such as hydrogen bonding or electronic coupling between g-C_3N_4 and $BiVO_4$, which play a significant role in enhancing photocatalytic performance by promoting charge transfer across the heterojunction.

These FTIR data are consistent with the results of XRD analysis, which show a weakening and broadening of the diffraction peaks of $BiVO_4$ after composite formation with g-C_3N_4. In the XRD data, the weakening of the intensity of the diffraction peaks of the $BiVO_4$ crystal planes (such as in the (121) and (040) planes) indicates that the integration of g-C_3N_4 into the $BiVO_4$ matrix caused a slight disturbance in its crystal structure. Peak intensity weakening also observed in the FTIR data, where the peaks of $BiVO_4$ remain visible, but with a slightly weaker intensity due to inter-molecular interactions. The analysis of FTIR and XRD data indicates that the formation of $BiVO_4$-NS/g-C_3N_4 composite improves the distribution of interactions between $BiVO_4$ and g-C_3N_4, potentially enhancing the photocatalytic activity. The strong C=N and C-N groups of g-C_3N_4 play an essential role in enhancing the electron transfer efficiency, while $BiVO_4$ still provides the active centre for the photocatalytic reaction.

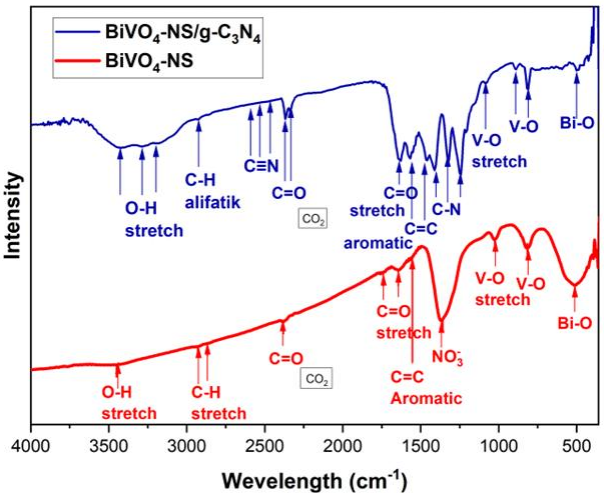

Figure 2. FTIR Spectra of $BiVO_4$-NS and $BiVO_4$-NS/g-C_3N_4 composites.

3.3 Morphological Characterization of $BiVO_4$-NS/g-C_3N_4

The results of scanning electron microscope analysis (Figure 3) show the morphological characteristics of $BiVO_4$, $BiVO_4$-NS, g-C_3N_4, and $BiVO_4$-NS/g-C_3N_4 composite materials. In the g-C_3N_4 material, the observed morphology shows an irregular layered structure with overlapping layers (Fig 3D). This structure is characteristic of graphitic carbon nitride, which has a two-dimensional planar nature with bonding between layers by van der Waals forces. This morphology provides a high surface area, allowing good contact between the material and the target molecules during the photocatalytic process. However, the relatively low degree of crystallinity of g-C_3N_4 can limit the charge transfer efficiency during the reaction [21].

For $BiVO_4$-NS material, SEM image shows a rectangular rod-like structure with a relatively large particle size [22]. This structure indicates directed and controlled crystal growth, supporting the monoclinic phase characteristics of $BiVO_4$. The smooth surface of the $BiVO_4$-NS crystals indicates a high purity of the material, most likely achieved by reasonable pH control during the synthesis process. However, the larger particle size may negatively impact the specific surface area, and particle aggregation could diminish the material's efficiency in certain applications. In contrast, pure $BiVO_4$ typically exhibits a sphere-grape-like morphology, characterized by rounded, clustered particles with generally smooth surfaces. This spherical aggregation suggests less directional crystal growth and possibly a higher degree of agglomeration, which may influence photocatalytic activity and surface interaction differently compared to the rod-like $BiVO_4$-NS. The transformation of $BiVO_4$ morphology from spherical to rod-like upon the addition of NS extract may be attributed to the role of NS as a

natural structure-directing agent. Bioactive compounds present in the extract, such as flavonoids and phenolic compounds, can interact with the metal precursors during the synthesis, altering the nucleation and growth kinetics of the crystals. These interactions promote anisotropic crystal growth, leading to the formation of a rod-like morphology instead of isotropic spherical particles. Moreover, the organic molecules in NS may act as capping agents, selectively adsorbing on specific crystal facets and thus directing the crystal growth in a particular orientation. This suggests that NS not only influences the purity and crystallinity of $BiVO_4$ but also plays a key role in tailoring its morphology, which in turn can affect its photocatalytic performance.

The $BiVO_4$-NS/g-C_3N_4 composite shows a unique blend of the morphologies of both materials. SEM results show the rod structure of $BiVO_4$-NS fused with the irregular g-C_3N_4 layer, indicating good contact between the two materials. The presence of these two materials in one composite enables the formation of an effective heterojunction, which can accelerate the separation process of electron-hole pairs during photocatalytic reactions.

SEM analysis results show that the $BiVO_4$-NS/g-C_3N_4 composite successfully combines the advantages of each material, namely the good surface area of g-C_3N_4 and the high visible light absorption capability of $BiVO_4$-NS. In addition, the uniform particle distribution in the composite indicates a synergistic interaction between the two materials, which can improve the charge transfer efficiency by forming an effective heterojunction to minimize the recombination of electron-hole pairs. The morphology of the g-C_3N_4 layer surrounding the $BiVO_4$-NS particles also provides better structural stability by preventing particle agglomeration while creating more active sites on the material surface. This allows for more effective interactions with target molecules, such as pollutants, improving photocatalytic efficiency. In addition, the combination of the layered morphology of g-C_3N_4 and $BiVO_4$-NS rod particles improves the optical properties of the material, allowing it to absorb and reflect visible light optimally. The presence of the g-C_3N_4 layer also provides additional protection against material degradation due to aggressive reaction environments, increasing the durability of the composite in long-term applications. With these

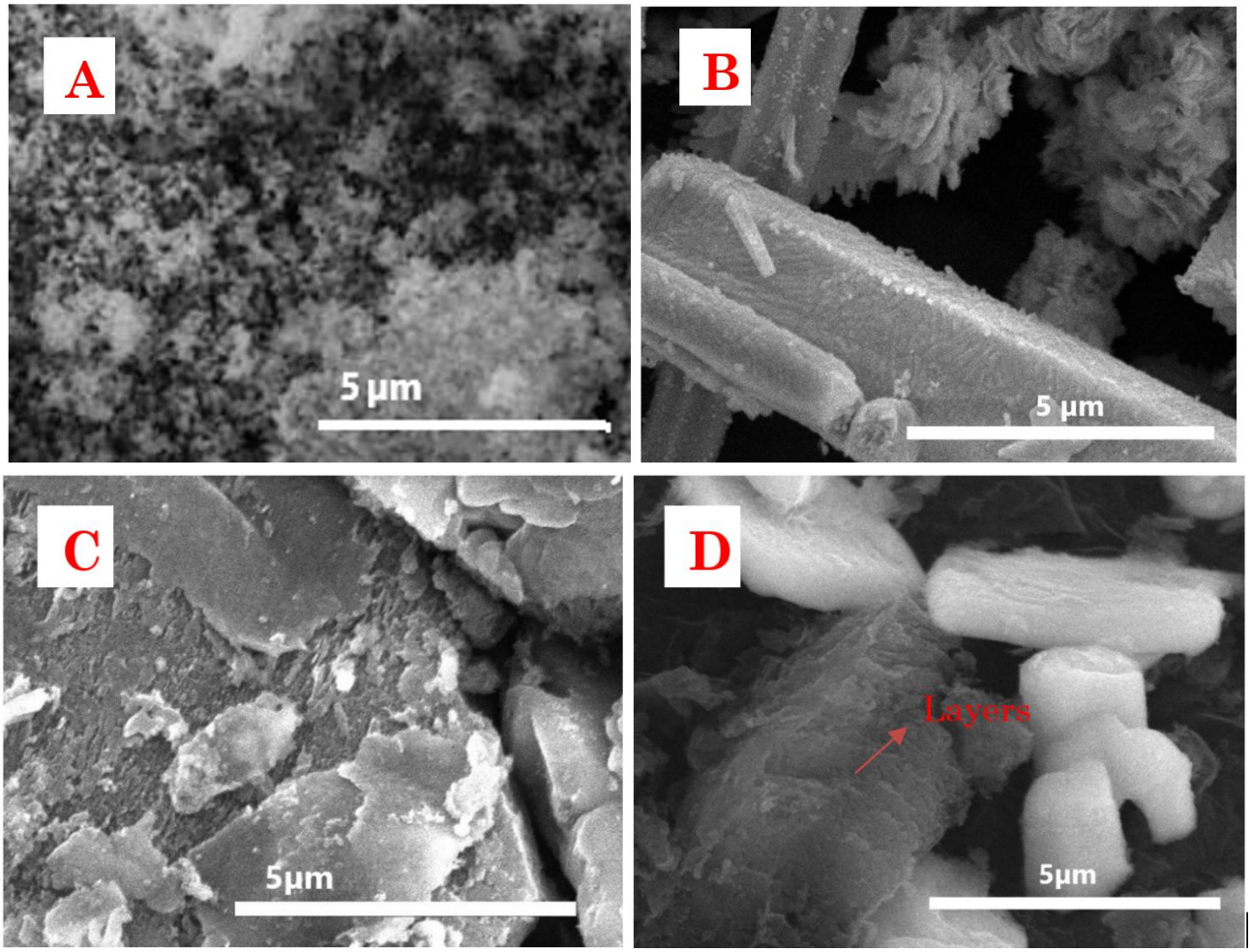

Figure 3. SEM images of $BiVO_4$ (A), $BiVO_4$-NS (B), g-C_3N_4 (C), and $BiVO_4$-NS/g-C_3N_4 composites (D).

various advantages, $BiVO_4$-NS/g-C_3N_4 has excellent potential for use in photocatalytic applications such as pollutant degradation or other chemical reactions that require high efficiency under visible light irradiation.

3.4 BET Surface Area and Porosity Analysis

The BET analysis results shown in Figure 4 for the $BiVO_4$-NS/g-C_3N_4 sample indicate that the nitrogen adsorption-desorption isotherm curve belongs to type IV, which is typical for materials with mesoporous structure (pore diameter 2-50 nm). The presence of significant hysteresis at relatively high pressures ($P/P_0 > 0.8$) indicates the presence of a pore system with good interconnection, which is common in composite materials. This phenomenon reflects the ability of the material to reversibly absorb and release gas in sufficiently large pores, supporting the diffusion of target molecules such as organic pollutants or water molecules in photocatalytic applications [23]. It is also shown that the synthesis strategy based on NS and g-C_3N_4 successfully produces materials with efficient pore structures without losing the structural integrity of $BiVO_4$ as the main photocatalyst.

The pore size distribution analyzed by the Barrett-Joyner-Halenda (BJH) method shows a significant peak at an effective diameter of 3.826 nm, confirming that mesoporous pores dominate this material. Pores in this size range are ideal for photocatalytic applications as they allow the absorption of organic molecules such as dyes, phenolic compounds, or small to medium-sized gases. These pores create an optimal diffusion path that not only facilitates the uptake of target molecules onto the active surface but also allows for the rapid release of degradation products. This feature minimizes the risk of catalytic inhibition caused by the accumulation of target molecules or reaction products within the pores. This is often a problem in materials with tiny pores.

The material-specific surface area of 24.098 m^2/g, although not very high compared to other mesoporous materials, is sufficient to support photocatalytic performance, especially considering the combination of pore size distribution and surface character. This surface area indicates that the synthesis of this composite has succeeded in creating a material with a sufficient number of active sites to support the interaction between the photocatalyst and the target molecules. In the context of photocatalytic applications, the combination of moderate surface area and optimal mesoporous structure is a key factor in optimizing degradation efficiency since the material depends not only on its surface area but also on the ability of its pores to provide accessibility to active sites. The BET characterization results show that $BiVO_4$-NS/g-C_3N_4 possesses porosity properties that are highly supportive for photocatalytic applications under visible light. The mesoporous structure increases the diffusion rate of target molecules towards the active surface, while the uniform pore size distribution helps to avoid inhibitory effects due to electron-hole recombination [24–26].

3.5 Optical Properties and Bandgap Determination

The DRS test results in Figure 5 show that the bandgap energy of the g-C_3N_4, $BiVO_4$-NS, and $BiVO_4$-NS/g-C_3N_4 composite samples varies significantly. The g-C_3N_4 material has a bandgap of 2.48 eV, which reflects its ability to absorb visible light at specific wavelengths. On the other hand, $BiVO_4$-NS has a smaller bandgap of 2.28 eV, which allows it to absorb a broader spectrum of visible light. This smaller bandgap is due to the electronic structure of the $BiVO_4$ material, which intrinsically has a higher valence band (VB) energy level due to the contribution of 6s orbitals from Bi^{3+} ions. However, like g-C_3N_4, $BiVO_4$ also has limitations in charge transfer due to the low charge carrier mobility.

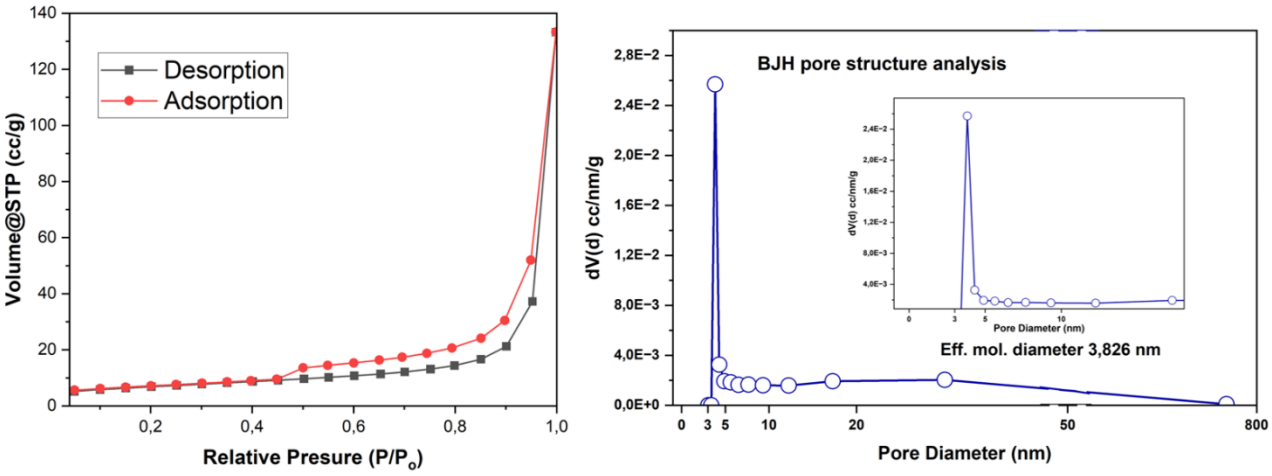

Figure 4. BET and pore structure analysis of $BiVO_4$-NS/g-C_3N_4 composite.

In the $BiVO_4$-NS/g-C_3N_4 composite, there is a decrease in the bandgap value compared to the single material, with the lowest value recorded at a ratio of 1:2 (2.13 eV). This decrease can be explained by forming a type-II heterojunction between the two materials. In a type-II heterojunction, the energy levels of the conduction band (CB) and valence band (VB) of both materials are arranged in such a way as to allow electron transfer from the g-C_3N_4 conduction band to the $BiVO_4$-NS conduction band. Conversely, holes from the valence band of $BiVO_4$-NS can transfer to the valence band of g-C_3N_4. This process creates more efficient charge separation, reduces the recombination rate of electron-hole pairs, and improves photocatalytic performance [27].

In addition, chemical interactions at the interface between $BiVO_4$-NS and g-C_3N_4, such as hydrogen bonding or electrostatic interactions, create new interface energy levels. These energy levels narrow the effective bandgap of the composite, which explains the decrease in bandgap value compared to single materials. The electron density adjustment due to the presence of $BiVO_4$-NS can also change the charge distribution on g-C_3N_4, broadening the visible light absorption spectrum. This increases electron excitation, which is essential in the photocatalytic process.

The ratio between $BiVO_4$-NS and g-C_3N_4 affects the efficiency of the synergistic formed. At a ratio of 1:2, a higher proportion of g-C_3N_4 material provides a sufficient number of active sites to create a strong interaction with $BiVO_4$-NS, thereby increasing the charge transfer efficiency. However, at higher ratios (1:3 and 1:4), the dominance of $BiVO_4$-NS reduces the proportion of interaction with g-C_3N_4 so that the bandgap value of the composite is closer to that of $BiVO_4$-NS. This shows that the optimum ratio of the composite occurs at 1:2, where the synergistic interaction between the two materials is at its maximum.

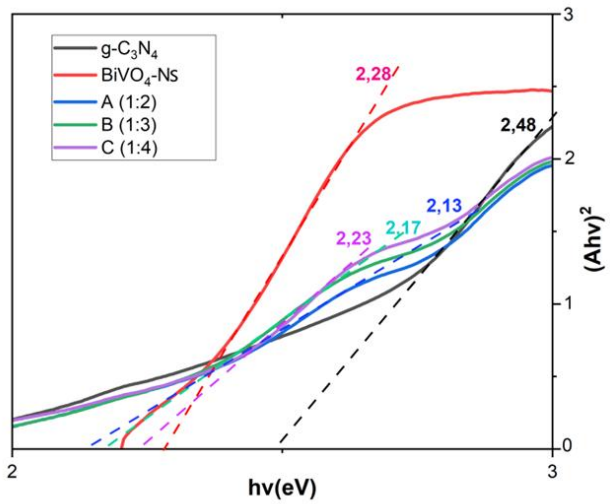

Figure 5. The band gap energy of $BiVO_4$-NS and $BiVO_4$-NS/g-C_3N_4 composites.

The decrease of bandgap in the composite indicates that this material can absorb more visible light than the single material, enhancing electron excitation, which plays an essential role in the photocatalytic process. These overall results indicate that $BiVO_4$-NS/g-C_3N_4 composites, especially at a 1:2 ratio, have great potential in visible light-based photocatalytic applications, with the interaction mechanism favouring better charge transfer efficiency and electron-hole pair separation.

3.6 Optimization of Mass for Enhanced Degradation Efficiency

In this study, the $BiVO_4$-NS/g-C_3N_4 composite was tested for its performance in methylene blue degradation with variations in mass ratio (1:2, 1:3, and 1:4). The results in Figure 6 show that sample A (1:2) gave the most optimal performance with a total removal of 91.73%. This performance was supported by a high adsorption activity of 81.12%, while the photocatalytic activity was at 10.60%. The dominance of adsorption activity in sample A indicates that g-C_3N_4 plays an essential role in capturing methylene blue molecules through physicochemical interaction mechanisms. Carbon-based materials such as g-C_3N_4 have a large surface area and good porosity, allowing effective interaction with methylene blue molecules through hydrogen bonding, van der Waals forces, or π-π interactions between the aromatic ring of methylene blue and the surface of g-C_3N_4 [28]. In addition, the presence of functional groups such as amines and imines on the g-C_3N_4 surface favours electrostatic interactions with dye molecules. This interaction results in a high concentration of Methylene Blue molecules around the composite surface, which indirectly increases the efficiency of the photocatalytic process.

Although the photocatalytic activity of sample A is lower than its adsorption activity, the presence of $BiVO_4$-NS still makes an essential contribution to the degradation of methylene blue. As a semiconductor, $BiVO_4$-NS can absorb visible light and produce electron-hole pairs (e^--h^+) when exposed to light. Electrons (e^-) formed in the conduction band react with oxygen (O_2) to form superoxide radicals (O_2^-). In contrast, holes (h^+) in the valence band can oxidize water molecules into hydroxyl radicals (-OH) [29]. These two reactive oxygen species (ROS) are very effective in breaking the chemical bonds in the methylene blue molecule, which ultimately decomposes it into simpler compounds. In sample A, the good balance between the adsorption surface area of g-C_3N_4 and the ability of $BiVO_4$-NS to generate ROS was the main factor supporting the high

degradation performance. In contrast, in samples B (1:3) and C (1:4), the total degradation decreased to 88.40% and 85.29%, respectively, although the photocatalytic activity slightly increased, which was 17.74% in B and 16.14% in C. The reduced adsorption activity can be due to the agglomeration of $BiVO_4$-NS/g-C_3N_4 at a higher mass ratio. Increasing the mass of g-C_3N_4 tends to block the active area of the composite surface, thus reducing the number of adsorbed methylene blue molecules. In addition, excess g-C_3N_4 can produce a screening effect, which blocks the penetration of light to $BiVO_4$-NS, thereby reducing the efficiency of electron excitation and increasing the recombination rate of electron-hole pairs.

Overall, the interaction between g-C_3N_4 and $BiVO_4$-NS in these composites creates an effective heterojunction capable of favoring the separation of electron-hole pairs and prolonging the lifetime of the generated ROS species. However, this phenomenon is only optimal at a particular mass ratio in sample A (1:2). Thus, the balance between adsorption surface area and photocatalytic efficiency becomes a key factor in determining the degradation performance. The findings of this study highlight the significance of designing composites that account for both adsorption capacity and photocatalytic ability to enhance overall degradation efficiency.

3.7 Impact of pH on Degradation Efficiency Optimization

The effect of pH on the photocatalytic performance of $BiVO_4$-NS/g-C_3N_4 composite in Figure 7 showed that alkaline pH (pH of 9-10) gave the highest methylene blue degradation efficiency, reaching more than 96%, while at low pH (pH of 3-5) the degradation efficiency was much lower. These results are closely related to the material properties of $BiVO_4$ and g-C_3N_4 and their response to acidic and alkaline environmental conditions, as well as the role of NS used as a solvent in the synthesis of $BiVO_4$. $BiVO_4$, with its monoclinic structure and narrow band gap energy (2.4 eV), is stable in neutral to alkaline environments. However, under acidic conditions, the surface of $BiVO_4$ tends to be protonated, generating a positive charge that causes electrostatic repulsion with positively charged methylene blue molecules. This decreases the dye adsorption efficiency on the photocatalyst surface and inhibits the transfer of molecules to the active site. Furthermore, the acidic environment restricts the formation of reactive oxygen species (ROS), such as hydroxyl radicals (·OH), due to insufficient concentration of OH- ions necessary for reacting with holes (h+) in the valence band of $BiVO_4$ [19-30]. In contrast, at alkaline pH, the $BiVO_4$ surface is negatively charged due to the adsorption of OH- ions, which facilitates electrostatic interaction with methylene blue and favours the formation of ROS, including ·OH radicals and superoxide radicals (O_2^-). This accelerates the degradation of Methylene Blue.

The g-C_3N_4 material also contributes significantly to the performance of the composite, especially in alkaline environments. Under alkaline conditions, the pores of g-C_3N_4 become more extensive, increasing the specific surface area and the number of active sites available for photocatalytic reactions [20]. In addition, the abundant OH^- ions under alkaline conditions favor the formation of ROS and enhance the electron transfer from g-C_3N_4 to $BiVO_4$-Nigella Sativa across the composite interface. This electron transfer prevents the recombination of electron-hole pairs (e^-/h^+), prolongs the lifetime of

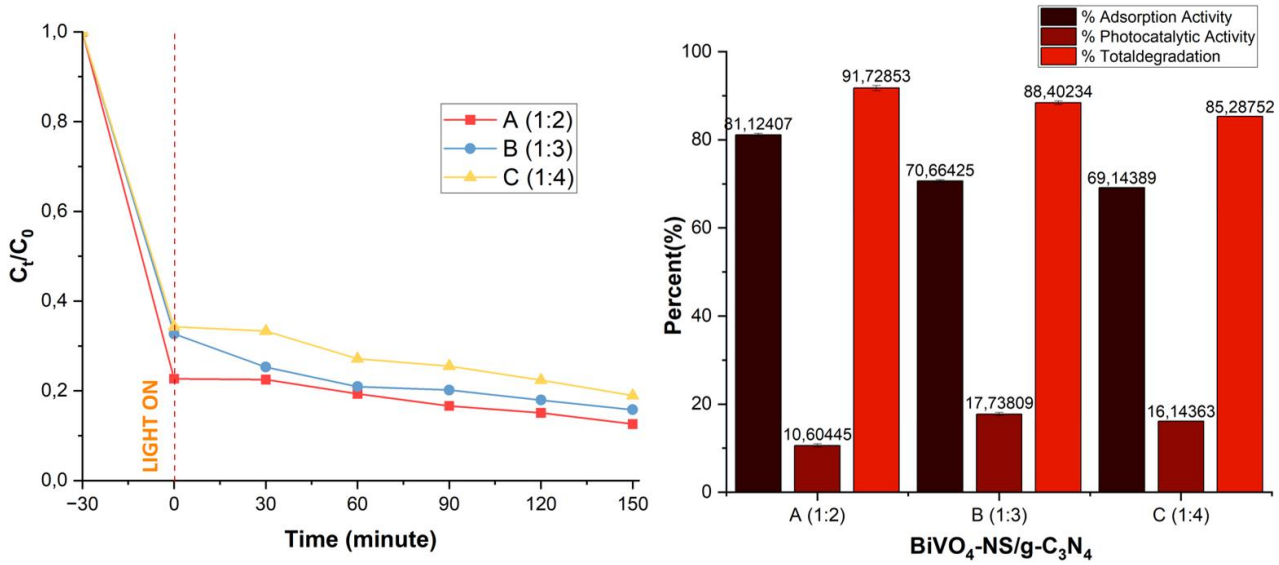

Figure 6. The effect of volume variation of mass ratio of $BiVO_4$-NS/g-C_3N_4 composites on MB photodegradation.

active ROS species, and improves the degradation efficiency of methylene blue. Thus, the synergistic interaction between $BiVO_4$-NS and g-C_3N_4 in an alkaline environment resulted in high degradation efficiency.

NS, although used as a solvent in the synthesis of $BiVO_4$, can affect the final properties of the material. Active compounds in NS, such as polyphenols, can interact with the $BiVO_4$ precursor during the synthesis process, helping to create a more ordered morphology or structure of the material [21]. This resulting structure contributes to the adsorption efficiency of methylene blue and the transfer of molecules to active sites in the photocatalytic reaction. At alkaline pH, the optimal synergistic interaction between $BiVO_4$, g-C_3N_4, and the influence of NS on the material results in maximum photocatalytic activity. In contrast, less favorable electrostatic interactions at low pH, limited ROS formation, and low molecular transfer efficiency lead to suboptimal photocatalytic performance. These findings underscore the significance of pH in optimizing the performance of $BiVO_4$-NS and g-C_3N_4-based photocatalysts, particularly in organic waste degradation. Based on these results, the selected $BiVO_4$-g-C_3N_4 composites were compared among various reported investigations on MB degradation which are summarized in Table 2.

4. Conclusion

In conclusion, this study on $BiVO_4$-Nigella Sativa/g-C_3N_4 composites demonstrates significant advancements in photocatalytic materials for dye degradation, specifically targeting methylene blue. The research identified an optimal mass ratio of 1:2, which resulted in a remarkable degradation efficiency of 91.73%. This high efficiency is attributed to the dominant adsorption process (81.12%) coupled with a notable photocatalytic activity of 10.60%. The findings highlight the critical role of material composition, as the incorporation of Nigella Sativa enhances the structural integrity and photocatalytic performance of the $BiVO_4$/g-C_3N_4 composites. The study further emphasizes that optimal degradation occurs under alkaline conditions (pH of 9-10), where enhanced reactive oxygen species (ROS) formation significantly contributes to the degradation process. XRD characterization confirmed the formation of a monoclinic structure of $BiVO_4$ and a stable $BiVO_4$-NS/g-C_3N_4 composite. SEM results showed

Table 2. Comparison between previous and current studies for MB removal using photocatalytic degradation.

Photocatalysts	Light source	Time (min)	Removal percentage (%)	Refs.
ZnO/Bentonite	UV	180	~71	[31]
$BiVO_4/NiFe_2O_4$	Visible	180	80	[32]
TiO_2/Fe_3O_4/GO	Visible	90	76	[33]
$WO_3/BiVO_4$/Graphene	Visible	120	63	[34]
g-C_3N_4/WO_3/rGO	Visible	180	76	[35]
g-$C_3N_4/BiVO_4$/NS	Visible	150	91	This work

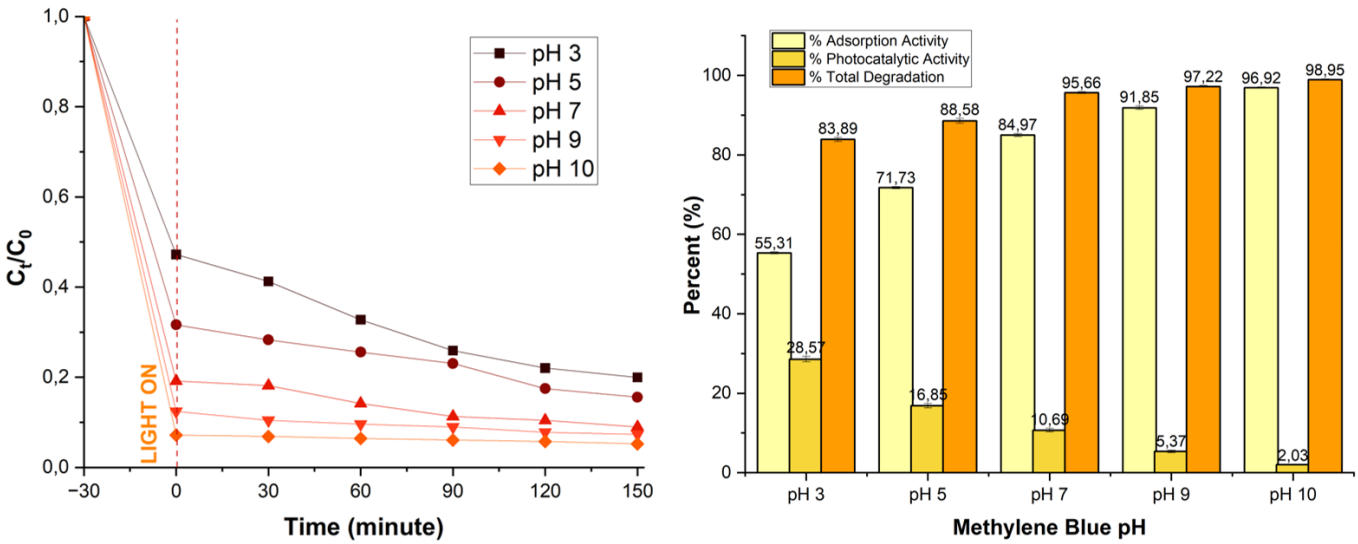

Figure 7. The effect of pH variation of $BiVO_4$-NS/g-C_3N_4 composites on MB photodegradation (blue light).

regular morphology with increased porosity, which supported the enhancement of active surface for adsorption and photocatalytic processes. FTIR and UV-Vis DRS showed a significant interaction between $BiVO_4$-NS and g-C_3N_4, which enhanced the separation of electron-hole pairs and prolonged the reactive life of the species, thus supporting more efficient methylene blue degradation. These findings are significant as they advance the development of eco-friendly photocatalytic systems for wastewater treatment, addressing a pressing environmental concern related to dye pollution. Future research directions should focus on optimizing synthesis parameters to further enhance the photocatalytic efficiency and stability of these composites. Additionally, exploring the integration of other natural materials and varying operational conditions could provide deeper insights into maximizing the performance of photocatalytic systems. This study lays a strong foundation for future investigations aimed at refining composite technologies and improving their applicability in real-world wastewater treatment scenarios.

Acknowledgement

The Institute for Research and Community Service of Jenderal Soedirman University supported this study under Riset Dasar Unsoed Grant, contract No. 27.157/UN23.37/PT.01.03/II/2023.

CRediT Author Statement

Author Contributions: A. Riapanitra: Conceptualization, Methodology, Investigation, Resources, Data Curation, Writing, Review and Editing, Supervision; G.H. Haryadinaru: Conceptualization, Formal Analysis, Data Curation, Writing Draft Preparation, Visualization, Software; T. Setyaningtyas: Project Administration, Methodology, Investigation, Review and Editing, Validation, Supervision. All authors have read and agreed to the published version of the manuscript.

References

[1] Riapanitra, A., Setyaningtyas, T., Haryadinaru, G.H. Photodegradation of Methylene Blue Dye Using $BiVO_4$/g-C_3N_4 Composites under Visible Light Irradiation. *Jurnal Kimia Sains dan Aplikasi*, 27(8), 363–370. DOI: 10.14710/jksa.27.8.363-370.

[2] Cai, H., Cheng, L., Chen, H., Dou, R., Chen, J., Zhao, Y., Li, F., Fang, Z. (2023). Facile phase control and photocatalytic performance of BiVO4 crystals for methylene blue degradation. *International Journal of Environmental Research and Public Health*, 20(4), 3093. DOI: 10.3390/ijerph20043093.

[3] Ni, S., Fu, Z., Li, L., Ma, M., Liu, Y. (2022). Step-scheme heterojunction g-C3N4/TiO2 for efficient photocatalytic degradation of tetracycline hydrochloride under UV light. *Colloids and Surfaces A: Physicochemical and Engineering Aspects*, 649, 129475. DOI: 10.1016/j.colsurfa.2022.129475.

[4] Mohamed, H.E.A., Sone, B.T., Khamlich, S., Coetsee-Hugo, E., Swart, H.C., Thema, T., Sbiaa, R., Dhlamini, M.S. (2021). Biosynthesis of BiVO4 nanorods using Callistemon viminalis extracts: Photocatalytic degradation of methylene blue. *Materials Today: Proceedings*, 36, 328–335. DOI: 10.1016/j.matpr.2020.04.119.

[5] Zhang, X., Li, M., Liu, C., Zhang, Z., Zhang, F., Liu, Q. (2021). Enhanced the efficiency of photocatalytic degradation of methylene blue by construction of Z-scheme g-C3N4/BiVO4 heterojunction. *Coatings*, 11(9), 1027. DOI: 10.3390/coatings11091027

[6] Mohamed, H.E.A., Sone, B.T., Dhlamini, M.S., Maaza, M. (2018). Bio-synthesis of BiVO4 Nanorods Using Extracts of Callistemon viminalis. *MRS Advances*, 3(42), 2479–2486. DOI: 10.1557/adv.2018.318.

[7] Rahim, M.A., Shoukat, A., Khalid, W., Ejaz, A., Itrat, N., Majeed, I., Koraqi, H., Imran, M., Nisa, M.U., Nazir, A. (2022). A narrative review on various oil extraction methods, encapsulation processes, fatty acid profiles, oxidative stability, and medicinal properties of black seed (Nigella sativa). *Foods*, 11(18), 2826. DOI: 10.3390/foods11182826.

[8] Elsayed, H., Mohamed, A., Afridi, S., Khalil, A.T., Zohra, T., Alam, M.M., Ikram, A., Shinwari, Z.K., Maaza, M. Phytosynthesis of BiVO4 nanorods using Hyphaene thebaica for diverse biomedical applications. *AMB Express*, 9, 200, 1-14. DOI: 10.1186/s13568-019-0923-1

[9] Zhu, B., Cheng, B., Fan, J., Ho, W., Yu, J. (2021). g-C3N4-based 2D/2D composite heterojunction photocatalyst. *Small Structures*, 2(12), 2100086. DOI: 10.1002/sstr.202100086.

[10] Goktas, S., Goktas, A. (2021). A comparative study on recent progress in efficient ZnO based nanocomposite and heterojunction photocatalysts: A review. *Journal of Alloys and Compounds*, 863, 158734. DOI: 10.1016/j.jallcom.2021.158734.

[11] Mu, F., Xu, S., Li, M., Yang, Y., Chu, X., Cheng, Z., Guo, X., Xu, J., Dai, B., Lee, C.-H. (2024). Photocatalytic peroxydisulfate activation for dissolved organic matter degradation in eutrophic lake water using S-scheme BiVO4/g-C3N4 3D/2D heterojunction under visible light. *Surfaces and Interfaces*, 48, 104382. DOI: 10.1016/j.surfin.2024.104382.

[12] Tran, T.-H., Le, P.-N.-M., Ngo, T.-H., Huynh, N.-D.-T., Oh, W.-C., Le, M.-V. (2024). An investigation on the visible light-driven Z-scheme BiVO4/g-C3N4 heterostructures: Performance, evaluation, and mechanism for dye and antibiotics degradation. *Materials Today Communications*, 40, 109373. DOI: 10.1016/j.mtcomm.2024.109373.

[13] Shakir, I. (2024). Tungsten-doped BiVO4 and its composite with g-C3N4 for enhanced photocatalytic applications. *Optical Materials*, 150, 115214. DOI: 10.1016/j.optmat.2024.115214.

[14] Akechatree, N., Rajendran, R., Rojviroon, T., Arumugam, P., Vasudevan, V., Sirivithayapakorn, S., Dhayalan, A., Wongpipun, P., Phetyim, N., Rojviroon, O. (2025). Development of Z-scheme BiVO4/g-C3N4/rGO heterojunction nanocomposite for enhanced photocatalytic degradation and antibacterial activity. *Materials Research Bulletin*, 181, 113119. DOI: 10.1016/j.materresbull.2024.113119.

[15] Vo, T.-G., Kao, C.-C., Kuo, J.-L., Chiu, C., Chiang, C.-Y. (2020). Unveiling the crystallographic facet dependence of the photoelectrochemical glycerol oxidation on bismuth vanadate. *Applied Catalysis B: Environmental*, 278, 119303. DOI: 10.1016/j.apcatb.2020.119303.

[16] Rathi, G., Siddiqui, S.I., Pham, Q., Nam, V.T. (2020). Nigella sativa seeds based antibacterial composites: A sustainable technology for water cleansing-A review. *Sustainable Chemistry and Pharmacy*, 18, 100332. DOI: 10.1016/j.scp.2020.100332.

[17] Algethami, J.S., Hassan, M.S., Amna, T., Alqarni, L.S., Alhamami, M.A.M., Seliem, A.F. (2023). Bismuth vanadate decked polyaniline polymeric nanocomposites: The robust photocatalytic destruction of microbial and chemical toxicants. *Materials*, 16(9), 3314. DOI: 10.3390/ma16093314.

[18] Yu, D., Xiong, Y., Wu, H., Yang, P., Shi, H., Huang, L., Wu, Y., Zhang, Y., Xiao, P. (2023). Chemical Bond-Modulated Interfacial Energy Band Structures of Heterojunctions for Efficient Photoelectrochemical Water Splitting. *The Journal of Physical Chemistry C*, 127(5), 2340–2348. DOI: 10.1021/acs.jpcc.2c08448.

[19] Devi, S., Kumar, S., Devi, J., Sharma, A., Kumar, A. (2023). Decoration of 1, 3 oxazole modified g-C3N4 by Bio-synthesized Ag nanoparticle for the photodegradation of pharmaceutical effluent: clotrimazole. *Mater. Today Proc.* Article In Press

[20] Ghotekar, S., Pagar, K., Pansambal, S., Murthy, H.A., Oza, R. (2020). A review on eco-friendly synthesis of BiVO4 nanoparticle and its eclectic applications. *Advanced Journal of Science and Engineering*, 1(4), 106–112. DOI: 10.22034/AJSE2014106.

[21] Yu, Y., Huang, H. (2023). Coupled adsorption and photocatalysis of g-C3N4 based composites: material synthesis, mechanism, and environmental applications. *Chemical Engineering Journal*, 453, 139755. DOI: 10.1016/j.cej.2022.139755.

[22] Sharma, K., Kumar, A., Ahamad, T., Alshehri, S.M., Singh, P., Thakur, S., Van Le, Q., Wang, C., Huynh, T.-T., Nguyen, V.-H. (2022). Improving the redox performance of photocatalytic materials by cascade-type charge transfer: a review. *Environmental Chemistry Letters*, 20(5), 2781–2795. DOI: 10.1007/s10311-022-01466-1.

[23] Majdoub, M., Anfar, Z., Amedlous, A. (2020). Emerging chemical functionalization of g-C3N4: covalent/noncovalent modifications and applications. *ACS Nano*, 14(10), 12390–12469. DOI: 10.1021/acsnano.0c06116.

[24] Ong, W.-J., Shak, K.P.Y. (2020). 2D/2D Heterostructured Photocatalysts: An Emerging Platform for Artificial Photosynthesis. *Solar RRL*, 4(8), 2000132. DOI: 10.1002/solr.202000132.

[25] Huang, X., Shen, T., Zhang, T., Qiu, H., Gu, X., Ali, Z., Hou, Y. (2020). Efficient Oxygen Reduction Catalysts of Porous Carbon Nanostructures Decorated with Transition Metal Species. *Advanced Energy Materials*, 10(11), 1900375. DOI: 10.1002/aenm.201900375.

[26] Zhan, W., Yuan, Y., Sun, L., Yuan, Y., Han, X., Zhao, Y. (2019). Hierarchical NiO@N-Doped Carbon Microspheres with Ultrathin Nanosheet Subunits as Excellent Photocatalysts for Hydrogen Evolution. *Small*, 15(22), 1901024. DOI: 10.1002/smll.201901024.

[27] Sharma, K., Vaya, D., Prasad, G., Surolia, P.K. (2023). Photocatalytic process for oily wastewater treatment: A review. *International Journal of Environmental Science and Technology*, 20(4), 4615–4634. DOI: 10.1007/s13762-021-03874-2.

[28] Wen, Y., Wang, Z., Cai, Y., Song, M., Qi, K., Xie, X. (2022). S-scheme BiVO4/CQDs/ß-FeOOH photocatalyst for efficient degradation of ofloxacin: Reactive oxygen species transformation mechanism insight. *Chemosphere*, 295, 133784. DOI: 10.1016/j.chemosphere.2022.133784.

[29] Dong, J., Zhang, Y., Hussain, M.I., Zhou, W., Chen, Y., Wang, L.-N. (2021). g-C3N4: properties, pore modifications, and photocatalytic applications. *Nanomaterials*, 12(1), 121. DOI: 10.3390/nano12010121.

[30] Bazgir, H., Issaabadi, Z., Arabi, H. (2023). Green Nanomaterials as Photocatalyst/Catalyst: Exploration of Properties. In: *Handbook of Green and Sustainable Nanotechnology: Fundamentals, Developments and Applications*. Springer, pp. 973–1003. DOI: 10.1007/978-3-031-16101-8_20.

[31] Zulkarnain, Hakim, Y.M., Melwita, E., Mohadi, R. (2024). The Effects of Hydrothermal Temperatures on ZnO-Bentonite Composite Synthesis on Adsorption and Photodegradation of Methylene Blue Dye. *Science and Technology Indonesia*, 9(4), 1033–1041. DOI: 10.26554/sti.2024.9.4.1033-1041.

[32] Remlalfaka, W., Murugesan, C., Anantharamaiah, P.N., Prabu, N.M. (2021). Fabrication of magnetically recoverable BiVO4/NiFe2O4 composites for the photocatalytic degradation of methylene blue. *Ceramics International*, 47(8), 11526–11535. DOI: 10.1016/j.ceramint.2020.12.281.

[33] Nadimi, M., Ziarati Saravani, A., Aroon, M.A., Ebrahimian Pirbazari, A. (2019). Photodegradation of Methylene Blue by a Ternary Magnetic TiO2/Fe3O4/Graphene Oxide Nanocomposite under Visible Light. *Materials Chemistry and Physics*, 225, 464–474. DOI: 10.1016/j.matchemphys.2018.11.029.

[34] Liaqat, M., Munir, R.M., Maryam, I., Iqbal, T., Afsheen, S., Nabi, A.G., Khan, R.R.M., El-marghany, A., Warad, I., Basit, A. (2024). Synthesis and Characterization of WO3/BiVO4/Graphene Ternary Nanocomposites for the Photodegradation of Methlyene Blue and Tetracycline. *Materials Chemistry and Physics*, 320(May), 129465. DOI: 10.1016/j.matchemphys.2024.129465.

[35] Waheed, Z., Ghazanfar, S., Usman, M., Asif, H.M., Tariq, M., Mahmood, K., Haider, A., Sirajuddin, M. (2023). Synthesis and Characterization of Ternary Composite g-C3N4-WO3/rGO for Photocatalytic Activity in Degradation of Methylene Blue. *Bulletin of the Chemical Society of Ethiopia*, 37(5), 1123–1131. DOI: 10.4314/bcse.v37i5.5.